Submitted to Physical Review

UCRL-18879
Preprint

eq 2

PRODUCTION AND NEUTRAL DECAY OF THE ETA MESON IN $\pi^- p$ COLLISIONS

W. Bruce Richards, Charles B. Chiu, Richard D. Eandi, A. Carl Helmholz, Robert W. Kenney, Burton J. Moyer, John A. Poirier, Robert J. Cence, Vincent Z. Peterson, Narender K. Sehgal, and Victor J. Stenger

May 1, 1969

AEC Contract No. W-7405-eng-48

eq 4

UCRL-18879

DISCLAIMER

PRODUCTION AND NEUTRAL DECAY OF THE ETA MESON IN $\pi^- p$ COLLISIONS*

W. Bruce Richards,† Charles B. Chiu,‡ Richard D. Eandi,**
A. Carl Helmholz, Robert W. Kenney, Burton J. Moyer,
and John A. Poirier††

Lawrence Radiation Laboratory
University of California
Berkeley, California

and

Robert J. Cence, Vincent Z. Peterson, Narender K. Sehgal,‡‡
and Victor J. Stenger

University of Hawaii
Honolulu, Hawaii

May 1, 1969

ABSTRACT

The reaction $\pi^- p \rightarrow \eta n$ has been observed through the decay mode $\eta \rightarrow 2\gamma$ at T_{π^-} = 592, 655, 704, 875, 975, 1117, and 1300 MeV. The detection apparatus was a cubic array of six steel-plate optical spark chambers that completely surrounded a liquid hydrogen target. We identified events attributed to the decay of an η by the large c.m. opening angle between the two showers generated in the steel plates by the decay photons.

We have calculated the total cross section for η production, which is proportional to the number of events under the large-angle peak in the opening-angle distribution. The total cross section rises steeply from threshold to a maximum of about 2.4 mb at 650 MeV, and then falls gradually to about 0.66 mb at 1300 MeV.

The differential cross section was obtained by taking the coefficients of a Legendre-polynomial fit to the angular distribution of bisectors of selected two-shower events, and converting them to the coefficients of the η c.m. angular distribution. The differential cross section is found to be isotropic at 592 MeV, to require terms through $P_2(\cos\theta_\eta)$ between 655 MeV and 975 MeV, and to have a forward peak fitted by terms through $P_3(\cos\theta_\eta)$ at 1117 MeV and through $P_4(\cos\theta_\eta)$ at 1300 MeV.

It is suggested that production at threshold is predominantly through an S state, with some P_1 and D_3 waves entering by 655 MeV. We suggest that all the absorption in the S_{11} π-N state can be explained by the η production.

I. INTRODUCTION

First observed in 1961,[1] the η meson is the most recently discovered meson that is stable against decay by the strong interaction. Early experiments[2] showed quantum numbers of the η to be

$$J^P I^G = 0^- 0^+.$$

Prior to the experiment reported here decay modes of the η had been established, but there existed only a few isolated measurements of its total production cross section in various reactions, and no significant differential cross-section determinations at all. Unusual behavior had been noticed in the total cross section for the reaction $K^- p \to \Lambda \eta$; namely, a value of $(500 \pm 150)\,\mu b$ at 20 MeV above threshold, falling to $(150 \pm 100)\,\mu b$ at 60 MeV above threshold.[3] In view of these observations, a systematic set of measurements of an η-baryon production cross section in some other initial channel seemed important.

It is also important to study the interaction of the η meson with nucleons. We chose to see if the total η production cross section in $\pi^- p \to \eta n$ also passes through the resonances in the same energy region. Such behavior would indicate that the excited nucleon isobar states can also decay through an η particle. Measurement of the differential cross section in this region should add considerably to the knowledge of the production process.

Systematic study of the ηN interaction can also give some insight into phenomena of πN elastic scattering near 600 MeV pion kinetic energy. Since πN scattering at this energy is highly absorptive, quantitative phase-shift analyses of the important angular momentum states have proved

complicated and have yielded conflicting results.[4-8] Although there is no guarantee that the coupling strengths will be the same, any S-matrix pole associated with a πN resonance must be shared with all communicating channels.[9] Because the major two-body channel that communicates with the isotopic spin 1/2 πN system around 600 MeV is ηn, it is possible that the existence and position of the resonances could be better analyzed in the ηn channel. Conversely, an enhancement in the πN cross section might be fundamentally a reflection of a strong interaction in the ηn system.

In this experiment, designed to study neutral final states of $\pi^- p$ interactions in the region of the 600- and 900-MeV peaks in the total cross section, we have measured the total and differential cross sections for the reaction $\pi^- p \rightarrow \eta n$ at seven different energies from threshold to 1300 MeV. Eta mesons were detected primarily by observing the decay mode $\eta \rightarrow 2\gamma$ in steel-plate spark chambers. Our results have been briefly reported previously.[10] In this paper, we give more details of the analysis and present final results. The thesis of one of us (W. B. R.) contains further details.[11]

Multishower events from this same run have provided data on the branching ratio $R = \Gamma(\eta \rightarrow 3\pi^0)/\Gamma(\eta \rightarrow 2\gamma)$. The result has been published,[12] but the method is briefly described in Sec. V.

II. EXPERIMENTAL APPARATUS AND PROCEDURE

The arrangement of our experimental apparatus, described in detail in previous papers on $\pi^- p \rightarrow \pi^0 n$,[13,14] is considered only briefly here. As shown in Fig. 1, six 38-gap steel-plate spark chambers formed the sides of a hollow cube enclosing a liquid hydrogen target at the center of a 1-m^3 cavity, providing a 4π solid angle detector for high energy photons. (The inclusion of top and bottom chambers proved important for maximum sensitivity to details of the η angular distribution.) The first four gaps of each chamber were made with aluminum plates having a low photon-conversion probability. These "gaps" provided a visual check against charged particles. The remaining 34 gaps were between 1/8-in.-thick steel plates.

Incoming pions were detected by scintillation counters M_1, M_2, and M_3. The signature of a neutral event in the counters was $M_1 M_2 M_3 A_{0-9}$. These events were photographed in the spark chambers in order to record the spatial location of cascade showers resulting from materialization of final-state photons.

According to a Monte Carlo study[14] of the conversion efficiency of the spark chamber system, the probability that both γ rays from an η event of the type chosen for analysis would materialize and produce $\geq$ three-spark showers in the chambers varied from 93% to 97% over the entire range of energies of the experiment. Thus we had high efficiency for detecting η mesons, via the decay $\eta \rightarrow 2\gamma$, as two-shower events. The opening angle between the two photons ($\pi^- p$ c.m. system) has a distribution strongly peaked at angles larger than is observed for similar peaking of $\pi^0 \rightarrow 2\gamma$ photons (see Fig. 2).

The procedure for detecting ηn final states therefore was to select two-shower events from the "η region" of opening angle.

III. ANALYSIS OF TWO-SHOWER EVENTS

A. First Selection of Events

The half million pictures taken during this experiment were scanned and measured by use of selection criteria and techniques already discussed in detail.[13,14] Briefly, two-shower events were accepted for further analysis when (a) each shower produced sparks in at least three of five consecutive gaps, (b) no sparks appeared in the first four gaps (the aluminum region), and (c) the event appeared to originate near the hydrogen target.

Because of multiple scattering of electrons, the showers did not necessarily point straight back to the point of origin in the hydrogen target. Hence in criterion (c) an event with long showers was accepted if the line of the shower made an angle of less than 12 deg with the line through the target center and the shower beginning; this cutoff was relaxed somewhat for shorter showers.

In a Monte Carlo calculation, it was determined that about 9% of the events would have at least one shower beginning in the aluminum region of the spark chambers, and would be thrown out by criterion (b) above. The data were corrected for this effect.

Data were taken both with and without liquid hydrogen in the target flask. Full-to-empty ratios were about 3:1 for counter data and 9:1 for acceptable two-shower events. Both groups of film were scanned and measured by using the same selection criteria. Thus properly normalized distributions based on the target-empty data could be subtracted from

target-full distributions to correct for stray interactions of the pion beam in the target structure.

B. Second Selection of Events

In the sample of good two-shower events, the η events were separated from the π^0 events (from $\pi^- p \rightarrow \pi^0 n$) by means of the distribution in opening angle of the two decay γ rays, in the $\pi^- p$ c.m. system. The probability distribution of the c.m. opening angle, ϕ, which follows simply from decay kinematics,[15] is

$$\frac{dn}{d\phi} = \frac{\cos(\phi/2)}{2\gamma^2\beta \sin^2(\phi/2)\left[\beta^2 - \cos^2(\phi/2)\right]^{1/2}}, \qquad (1)$$

where β is the c.m. velocity of the decaying meson, and $\gamma = (1 - \beta^2)^{-1/2}$. As seen by inspecting the denominator of Eq. (1), the most prominent feature of the distribution is a divergence at a minimum opening angle related to β by

$$\cos(\phi_{min}/2) = \beta . \qquad (2)$$

Because the c.m. velocity of a particle depends on its mass as well as momentum, the η events may be cleanly separated from the neutral pions arising from charge exchange. Mass values used in calculations were from a standard compilation.[16] Shown in Fig. 2 is the γ-γ opening-angle distribution obtained at $T_{\pi^-} = 1300$ MeV. Note the prominent π^0 peak at 23 deg and the η peak (see also expanded scale) at about 90 deg. For comparison, the opening angle distribution for $T_{\pi^-} = 704$ MeV is given in Fig. 4 of Ref. 13.

In order that the sample of η's be as clean as possible, only those events within a limited range of angles were used for analysis. (See Table I.)

C. Background Reactions

In Fig. 2, the shape of the peaks agrees closely with the theoretical distribution function of Eq. (1) after one has folded in the angular resolution of the detector system (1.5 to 3 deg), momentum spread of the incoming beam (±2.5%), and detection efficiency. In the "η region" the background consisted of (a) np recoils and (b) multi-γ two-shower events, and ranged from 8% to 30%. See Table II.

1. np Recoils

Usually the final-state neutron is not detected, but occasionally it produces a visible charged knock-on (np recoil). Low energy, short-range proton tracks were difficult to distinguish visually from short electron showers. Hence, some true two-shower events appeared to be "three-shower" events. Kinematic fitting to the np recoil hypothesis showed that 5% of the η events included an additional np recoil track. In addition, some apparent two-shower events were really one-shower π^0n events with an np recoil. These latter tended to lie near 180 deg in a "two-shower" opening-angle plot, because the single shower is almost always produced by a high energy photon traveling in almost the same direction as the π^0.

All possibly ambiguous two-shower events were tested for the probability that one track was an np recoil. If the calculated energy was low enough that it was reasonable that the photon had been missed, and if the length of the supposed proton track was in reasonable agreement with its predicted range, then it was considered an "np event." A distribution in opening angle of the two observed tracks is shown in Fig. 3.

2. Multiphoton ($> 3\gamma$) two-shower events

In addition to πN charge exchange and η production, other neutral-final-state reactions yielding two or more photons could still produce two-shower events if only two photons materialize into detectable showers:

(a) $\pi^- p \rightarrow 2\pi^0 n$,

(b) $\pi^- p \rightarrow 3\pi^0 n$,

(c) $\pi^- p \rightarrow \Lambda K^0$,

(d) $\pi^- p \rightarrow \omega n$.

In chambers with less than 100% detection efficiency, the above reactions can produce two visible showers part of the time. Since the background is rather small, it was sufficient to estimate the opening-angle distributions from the background reactions by Monte Carlo calculations. In these estimates, the calculated photon energy response of the chambers[14] was taken into account. Three-body Lorentz-invariant phase space (LIPS) was assumed for reaction (a), four-body LIPS for reaction (b), and a Λ c.m. angular distribution of $(1-0.8 \cos \theta_\Lambda)$ for reaction (c),[17] and, for lack of better information, phase space was used for reaction (d). As suggested by the five- and six-shower data in this experiment, in the final calculation reaction (b) was assumed to go through an intermediate η, which then decayed into three neutral pions. Results are shown in Fig. 3, for $T_{\pi^-} = 1300$ MeV. The normalization of various components is based on either known production cross sections or the fitting procedure described in the next section.

D. Eta Production Cross Section

The η production cross sections are derived from the opening-angle distributions through the observable ratio

$$r = \frac{f_\eta \, \sigma (\pi^- p \to \eta n)}{f_\pi \, \sigma (\pi^- p \to \pi^0 n)} , \tag{4}$$

where f_η is the branching ratio[16]

$$f_\eta = \frac{\Gamma (\eta \to 2\gamma)}{\Gamma (\eta \to \text{all decays})} = 0.38 \pm 0.02 \tag{5}$$

and f_π is the branching ratio[16]

$$f_\pi = \frac{\Gamma (\pi^0 \to 2\gamma)}{\Gamma (\pi^0 \to \text{all decays})} = 0.988. \tag{6}$$

The ratio r is the ratio of the number of $\eta \to 2\gamma$ events in the opening-angle plot (η region only) from η decay to the number of events due to π^0 decay, corrected for two-shower detection efficiencies in each case (see below). The quantity r is insensitive to the errors that arise in measuring the total neutrals cross section measured with counters, or in scanning and measuring two-shower events. The main errors arise from the estimation of the detection efficiency of the chambers and the contribution of background reactions.

Once r has been determined, it can be multiplied by the $\pi^- p \to \pi^0 n$ charge-exchange cross section, also measured in these experiments,[13] to yield the partial production cross section

$$\sigma_\eta (2\gamma) = f_\eta \, \sigma (\pi^- p \to \eta n). \tag{7}$$

To evaluate r the technique used was to determine the linear combination of opening-angle distributions for $\pi^0 \to 2\gamma$, $\eta \to 2\gamma$, and background which

best fitted the experimental distribution. These opening-angle distributions were in the form of histograms, calculated either directly or by Monte Carlo methods. For π^0 and η distributions, a numerical integration was done to fold the measurement error, momentum spread of the beam, and detection efficiency of the chambers into the theoretical distribution given by Eq. (1). The background distributions (see Fig. 3) were calculated as described in the immediately preceding section. The fitting procedure then yielded the relative normalization of the different reactions, with errors obtained from the error matrix.

The most significant background resulted from final states containing more than two photons. The shape of this background estimated by the Monte Carlo calculations was checked by comparison with an experimental distribution. For this purpose, events were selected from the experimental sample of three-shower events in which the shortest of the three showers was less than 3 in. long within the chamber. These short showers were considered to be "almost missing," and opening-angle distributions were made from the remaining two showers to simulate a background two-shower event. The background distribution calculated by the Monte Carlo method compared quite favorably to this experimental estimate.

To check the sensitivity of the results to the various assumptions, fits were also made with (a) a flat opening-angle background, (b) a background proportional to the sine of the opening angle, as would be expected for completely uncorrelated pairs of showers, and (c) no efficiency corrections to the π^0 and η opening-angle curves. In all cases the χ^2 showed that these were significantly poorer fits to the

data than the ones using the Monte Carlo estimates. In cases (a) and (b) the resulting value of the ratio r did not vary more than one standard deviation from the best fit. When no efficiency correction was used the fit was extremely poor.

The final results of the fitting, with all corrections, are given in Table II. Figure 4 is a graph of this partial η production cross section, $\sigma_\eta(2\gamma) = \sigma(\pi^- p \to \eta n;\ \eta \to 2\gamma) = f_\eta\, \sigma(\pi^- p \to \eta n)$, as a function of energy.

E. Differential Cross Section

Measurement of the angular positions of the two showers determines the direction of the decayed η to within one of two possible directions. Attempts to resolve this quadratic ambiguity by trying to determine the relative energies of the γ rays by spark counting did not succeed. Instead, a slightly less direct method of analysis was used. In the Appendix we derive the η angular distribution from the experimental distribution of the bisector between the two γ rays. Since it is necessary to have a 4π-sr detector to perform a direct conversion, our particular experimental arrangement is ideal for this analysis.

To summarize the method, if the distribution of the bisectors is fitted by a sum of Legendre polynomials as

$$\left.\frac{d\sigma}{d\Omega}\right|_B = \sum_\ell A_\ell P_\ell(\cos\theta_B), \tag{8}$$

then the true η angular distribution is given by

$$\left.\frac{d\sigma}{d\Omega}\right|_\eta = \sum_\ell (A_\ell/\zeta_\ell) P_\ell(\cos\theta_\eta). \tag{9}$$

The A_ℓ are the coefficients of the bisector fit, and

$$\zeta_\ell = \int_{\mu_{min}}^{1} \frac{(1-\beta^2)\,\mu\, P_\ell(\mu)d\mu}{(1-\mu^2)^{1/2}\left\{1-\mu^2\beta^2\right\}^{3/2}}, \qquad (10)$$

where $\mu_{min} = \beta^{-1}\cos(\Phi_{max}/2)$, Φ_{max} is the upper limit of the opening-angle interval from which the sample was taken, and β is the c.m. velocity of the meson. The Appendix also contains a table of values of ζ_ℓ as calculated by numerical integration for the energies of this experiment.

To form the angular distribution at each energy, two-shower events were selected within the opening-angle range given in Table I, and the direction of the bisector in the c.m. system was distributed in 10 bins of equal size in $\cos\theta_B$. Monte Carlo programs were also used to provide bisector distributions of background events. The primary background was from the $2\pi^0$n final state, and the approximate shape of the Monte Carlo bisector distribution for this reaction varied from $(1 - 0.14\cos\theta)$ to $(1-0.57\cos\theta)$ at the lowest and highest energies, respectively. Other backgrounds were essentially isotropic.

These Monte Carlo estimates of the background bisector distributions were compared with experimental distributions obtained from two of the three showers in the sample of three-shower events in which the third shower was very short. At low energies the angular distribution within the η region of the bisector of these "pseudo-two-shower events" compared very well with the Monte Carlo background calculation. However, at the highest two energies there were significantly fewer bisectors in the backward hemisphere in the "pseudo two-shower" sample than

the Monte Carlo calculation had predicted. The phase-space assumptions made in the Monte Carlo calculations become more liable to error as the energy increases. Since there was an adequate number of events in the experimental three-shower sample at the high energies, this experimental distribution was used instead of the Monte Carlo at T_{π^-} = 1117 and 1300 MeV.

Angular distributions are presented in Table III. The differential partial cross sections are normalized to the partial cross sections of Table II. Data points in Table III and Fig. 5 are the corrected experimental bisector distributions. The dotted lines in Fig. 5 are the best χ^2 fits to the bisector distribution. The coefficients of the Legendre polynomial expansion of this curve were then divided by the factors ζ_ℓ of Eq. (A-13) normalized in such a way that $\zeta_0 = 1$. The solid lines in Fig. 5 are plots of the new expansion, which represents the true η differential partial cross section $d\sigma_\eta(2\gamma)/d\Omega$ for the reaction $\pi^- p \rightarrow \eta n(\eta \rightarrow 2\gamma)$. Table IV and Fig. 6 contain the Legendre polynomial expansion coefficients of the η differential partial cross section, $\sigma_\eta(2\gamma)$.

Figure 7 shows the value of the parameter $(\chi^2/d)^{1/2}$ as a function of the order of fit for each energy. The choice of the best order of fit is sometimes ambiguous, but an advantage of a Legendre polynomial series over a cosine power series is that the conclusion about significant partial-wave components does not depend critically upon the order of fit within the ambiguous range.

IV. DISCUSSION OF RESULTS FOR CROSS SECTION AND ANGULAR DISTRIBUTIONS

The partial cross section for η production, $\sigma(\pi^- p \to \eta n;\ \eta \to 2\gamma)$, detected by the decay $\eta \to 2\gamma$, has been measured systematically over a broad range of pion energies by us and by another group.[18] The results are shown in Fig. 4. Note that the agreement is quite satisfactory at all energies, except perhaps near $T_{\pi^-} = 900$ MeV. Near 900 MeV, $\pi^0 n$ and $2\pi^0 n$ final states are so prominent that it becomes rather difficult to achieve clean separation of the η events from other two-shower events. This probably accounts for the scatter of points in this region. There is no definite evidence for structure in the η-production cross section above the 700-MeV peak.

If we take the branching ratio[16] $\Gamma(\eta \to 2\gamma)/\Gamma(\eta \to \text{all}) = 0.38$, the peak value of the cross section $\sigma(\pi^- p \to \eta n)$ becomes 2.44 mb. It is clear that η production is a significant inelastic channel.

The S-wave nature of $\pi^- p \to \eta n$ just above threshold is indicated by the shape of the cross-section curve. The combined data of Fig. 4 are fitted well by a linear dependence upon c.m. η momentum, up to $T_{\pi^-} = 650$ MeV ($p_\eta^* = 200$ MeV; see Fig. 44 of Ref. 11). A more detailed excitation function near threshold (15 MeV/c $< p_\eta^* <$ 113 MeV/c) has been made by others,[19] which confirms S-wave dominance near threshold. Our lowest-momentum point at $p_\eta^* = 116$ MeV/c is in excellent agreement with this work.[19]

The angular distributions observed[10,18,19] close to threshold are consistent with isotropy, at least below $T_\pi = 650$ MeV.

Phase-shift analyses of pion-nucleon scattering[4-8, 20, 21] have shown a strongly inelastic S_{11} ($T = 1/2$, $J = 1/2$) resonance near the threshold for η production ($T_\pi = 560$ MeV). Since the inelastic process $\pi^- p \to \eta n$ must be in the $T = 1/2$ state and is predominantly S-wave ($J = 1/2$) near threshold, it is of interest to see how much of the S_{11} inelasticity is accounted for by η production. Since the $\pi^- p$ initial state is $T = 1/2$ only 2/3 of the time,

$$\sigma_i(S_{11}) = 2/3\, \pi \lambda^2 \left[1 - b^2(S_{11})\right],$$

where $b(S_{11})$ is the inelasticity parameter for S_{11} state. Choosing a value of b from the pion-nucleon phase shifts of Bareyre,[5] and evaluating σ_i, one finds good agreement with the η-production cross section. The S_{11} inelasticity must then feed the ηn channel very strongly.[11]

Some authors[22-24] have attempted to fit $\sigma(\pi^- p \to \eta n)$ of Fig. 4 and various S_{11} phases by a two-channel scattering-length analysis using zero effective range. Uchiyama-Campbell[22] used the phase shifts of Auvil et al.[4] and obtained rather poor fits to the cross section, with no indication of an S_{11} resonance near threshold. Dobson[23] obtained a good fit to Cence's S_{11} phase shifts,[6] but the resulting η-production cross section rose too fast above threshold to fit the data of Fig. 4. No S_{11} resonance pole was indicated.

Ball[24] has used a dynamical model with two adjustable parameters to fit S-wave πN scattering and η-production data (see Fig. 4). His method shows a characteristic of the zero-range approximation in not fitting the lowest-energy points. This model also gives no S_{11} resonance pole.

Other authors[25,26] have shown that good fits are obtained by assuming a (Breit-Wigner type) S-wave N^*, $J^P = 1/2^-$ resonance dominating the ηn state near threshold. An effective-range K-matrix analysis[27] has also been used. A bound state at invariant mass of either 1530 MeV or 1570 MeV[26] is required, well above the threshold value of 1487 MeV.

The existence of other inelastic resonances in this region, particularly P_{11}(1460 MeV) and D_{13}(1515 MeV), leads to speculation concerning the decays of these resonances into the ηn final state. Davies and Moorhouse[28] and Moss[29] have included P_{11} and D_{13}, as well as S_{11}, resonances in their analyses and find that small amounts of these states improve the fit to the cross-section data. Only $\approx 4\%$ P and D waves is required at $T_\pi = 650$ MeV. The S_{11} resonance occurs consistently above threshold for η production.

Tripp's SU(3) considerations[30] predict a total contribution of ≤ 0.3 mb for each of the reactions $\pi^- p \to N^*_{1/2}(1680) \to \eta n$ and $\pi^- p \to N^*_{1/2}(1688) \to \eta n$. This cross-section contribution is clearly below our detection threshold.

The existence of P and D waves should be shown most directly in the angular distributions, as a departure from isotropy. Indeed, our data (Fig. 5) already show significant deviations from isotropy at $T_\pi = 655$ MeV, with a large $\cos^2\theta$ component. Linear ($\cos\theta$) and higher-order terms become prominent at increasing energy. The coefficients A_ℓ in the Legendre polynomial expansion of $d\sigma/d\Omega$ are plotted in Fig. 6. $A_3 \neq 0$ is required at $T_\pi = 873$ MeV and above. At the highest energy ($T_\pi = 1300$ MeV) $A_4 \neq 0$ is required. The minimum-order

fit required by the data is determined by plotting $(\chi^2/d)^{1/2}$ versus d, where d is the order of fit, as shown in Fig. 7. (The results of Ref. 18 are drawn from preliminary data, and are consistent with isotropy up to 1000 MeV. Final data, with extended statistics, of those authors, however, contain more complicated angular distributions, and there now exists substantial agreement between their final results and ours.[31])

The analysis by Davies and Moorhouse[28] has shown that excellent fits to the η-production data (Fig. 4), the angular distributions (Fig. 5), and the phase shifts of Bareyre et al.[5] can be obtained by assuming an S_{11} resonance (1534 MeV, total width 168 MeV) and a D_{13} resonance (1530 MeV, total width 65 MeV). The D wave contributes less than 10% to the cross section at the peak. A fairly substantial $\cos^2\theta$ term in the angular distribution is produced by interference of a small D-wave amplitude with a large S wave.

V. OTHER NEUTRAL ETA DECAYS: BRANCHING RATIO, $R = \Gamma(\eta \to 3\pi^0)/\Gamma(\eta \to 2\gamma)$

Eta production and neutral decay are most readily detected in our apparatus via the $\eta \to 2\gamma$ mode, due to the high conversion efficiency and unique opening-angle distribution of the decay photons. All the preceding data on differential cross sections for $\pi^- p \to \eta n$ are based on detecting this decay mode.

Multishower events (three or more showers) are also observed in significant numbers in our experiment, as shown in Table V. Such events arise from $2\pi^0 n$, $3\pi^0 n$, $\eta(\to 3\pi^0)n$, and $\eta(\to \pi^0\gamma\gamma)n$ final states. We have been able to derive approximate values for the production cross sections $\sigma(\pi^- p \to 2\pi^0 n)$, shown in Fig. 8, and $\sigma(\pi^- p \to 3\pi^0 n)$ and

we have obtained a value[12] for the branching ratio $R = \Gamma(\eta \to 3\pi^0)/\Gamma(\eta \to 2\gamma) = 1.1 \pm 0.2$. The development of a semi-empirical $\epsilon_1(k)$ for our chambers, using π^0 and $\eta(\to 2\gamma)n$ one-shower and two-shower events, has been discussed elsewhere.[13,14] The data at all nine incident π^- energies have been fitted with an $\epsilon_1(k)$ given by $\epsilon_1(k) = C\{1 - \exp[-(k-k_0)/\Delta k]\}$, where $k_0 = 15$ MeV, and where C varies between 0.95 and 1.00 while Δk varies from 60 to 85 MeV under different spark chamber conditions.

Detection of $3\pi^0 \to 6\gamma$ final states as "six-shower" events thus involves the sixfold product of such efficiency functions.

Detailed Monte Carlo calculations have been made[13,14] by using the above $\epsilon_1(k)$ to fit the estimated yields of $2\pi^0 n$ and $3\pi^0 n$ events to the observed shower distributions at each incident π^- energy. Phase-space distributions were assumed for the particles in $2\pi^0 n$ and $3\pi^0 n$ final states.

The results show good χ^2 fits to the observed shower-number distributions. The ratio of six-shower to five-shower events, which arise only from $3\pi^0 n$ or $\eta(\to 3\pi^0)n$ reactions, was fitted well with $\Delta k = 60 \pm 10$ MeV over the entire range of π^- energies[11] despite its sensitivity to the shape of $\epsilon_1(k)$. A problem arose in separating the last two modes. For $\eta(\to 3\pi^0)n$ two-body final-state Monte Carlo results, phase-space distributions for $\eta \to 3\pi^0$ resulted in shower distributions indistinguishable from the $3\pi^0 n$ four-body final state. This problem is tractable because of the abrupt rise in the number of five-shower and six-shower events about threshold for η production ($T_{\pi^-} = 560$ MeV). We have used this feature elsewhere[12] to separate $3\pi^0 n$ from $\eta(\to 3\pi^0)n$ final states, and to deduce $R = 1.1 \pm 0.2$. This implies a value of $\Gamma(\eta \to 3\pi^0)/\Gamma(\eta \to \pi^+\pi^-\pi^0) = 1.5 \pm 0.3$, consistent with pure

I = 1 final state in $\eta \rightarrow 3\pi$ decay. The decay $\eta \rightarrow \pi^0\gamma\gamma$ was not fully investigated, since it was clear that the $2\pi^0$n background was overwhelming in the absence of neutron detection or accurate photon energy information.

ACKNOWLEDGMENTS

We are indebted to Frederick A. Kirsten and Cordon R. Kerns for electronic design of certain critical circuits. We thank our scanning and measuring groups for their continued high quality efforts, which facilitated the successful completion of this experiment. We also thank the Bevatron staff under Walter D. Hartsough and the staff of the Computer Center for their excellent cooperation.

APPENDIX

A. Kinematics of Two-Gamma Decay

In this Appendix are derived the equations used in the analysis of η angular distributions, relating the distribution of the bisector of the γ rays (see Fig. 9-a) to the distribution of the η. The treatment of a neutral meson, η, with a 2γ decay mode, is in units where $c = 1$. All quantities are evaluated in the $\pi^- p$ c.m. frame.

Now we find an expression $d\sigma/d\Omega_B$ for the angular distribution of the bisectors, given the distribution in angle of the meson. First we put

$$\frac{d\sigma}{d\Omega_B} = \int \frac{d^2\sigma}{d\Omega_B d\Omega_\eta} \, d\Omega_\eta \, . \tag{A-1}$$

Here

$$\frac{d^2\sigma}{d\Omega_B d\Omega_\eta} \, d\Omega_B \, d\Omega_\eta$$

is the joint probability that an event occurs in which the η meson is in the element of solid angle $d\Omega_\eta$, and at the same time the bisector of the decay γ rays is in the solid angle $d\Omega_B$. The directions of the bisector and the incoming beam axis (from which the η production angles are measured) are held fixed, and the integration is over all possible directions of production of η.

The joint probability may be expressed

$$\frac{d^2\sigma}{d\Omega_\eta d\Omega_B} = \frac{d\sigma}{d\Omega_\eta} \cdot \frac{dn}{d\Omega_B} \, , \tag{A-2}$$

where

$$\frac{d\sigma}{d\Omega_\eta} \, d\Omega_\eta = \sum_\ell C_\ell P_\ell(\cos\theta_\eta) d\Omega_\eta \tag{A-3}$$

is the probability that an η appears in the solid angle $d\Omega_\eta$ at θ_η; and $(dn/d\Omega_B)d\Omega_B$ is the probability of finding the bisector in $d\Omega_B$ at the same time, a function of the angular separation δ of the η and the bisector. Thus, Eq. (A-1) is expanded to

$$\frac{d\sigma}{d\Omega_B} = \sum_\ell C_\ell \int P_\ell(\cos\theta_\eta) \frac{dn}{d\Omega_B} d\Omega_\eta . \qquad \text{(A-4)}$$

The choice of coordinate system in which to integrate cannot affect the result, so we choose the spherical coordinate system that has its polar axis in the direction of the bisector under consideration. This system is illustrated in Fig. 9-b.

Thus we have

$$\frac{d\sigma}{d\Omega_B} = \frac{1}{2\pi} \sum_\ell C_\ell \iint P_\ell(\cos\theta_\eta) \frac{dn}{d(\cos\delta)} d(\cos\delta)d\phi_\eta , \qquad \text{(A-5)}$$

where ϕ_η is the azimuthal angle of the η meson about the bisector as its polar axis. We can carry out the integration if we recall the addition theorem for spherical harmonics, which, for the vectors of Fig. 9-b,[32] can be written

$$P_\ell(\cos\theta_\eta) = P_\ell(\cos\delta)P_\ell(\cos\theta_B) + 2\sum_{m=1}^{\ell} \frac{(\ell-m)!}{(\ell+m)!} P_\ell^m(\cos\delta)P_\ell^m(\cos\theta_B)\times\cos\left[m(\phi_\eta-\phi_B)\right] . \qquad \text{(A-6)}$$

Again, ϕ_B is the azimuthal angle of the beam direction with respect to the bisector.

If we substitute this into Eq. (A-5), the integration over $d\phi_\eta$ can be done. All the terms in the expansion of $P_\ell(\cos\theta_\eta)$, except the

first, are multiplied by $\cos\,[m(\phi_\eta - \phi_B)\,]$, and these drop out when one integrates over $d\phi_\eta$ from 0 to 2π. After this step the bisector distribution is

$$\frac{d\sigma}{d\Omega_B} = \sum_\ell \left[C_\ell \int P_\ell(\cos\delta)\ \frac{dn}{d(\cos\delta)}\ d(\cos\delta)\right] P_\ell(\cos\theta_B). \qquad \text{(A-7)}$$

An expression for $dn/d(\cos\delta)$ is now required.

This distribution in the magnitude of the angle, δ, between the direction of the η meson and the bisector of the decay γ rays may be expressed

$$\frac{dn}{d\delta} = \frac{dn}{d\Phi} \cdot \frac{d\Phi}{d\delta}\,, \qquad \text{(A-8)}$$

where $dn/d\Phi$ is the well-known opening-angle distribution,

$$\frac{dn}{d\Phi} = \frac{1}{2\gamma^2\beta}\ \frac{\cos\Phi/2}{\sin^2\Phi/2\ (\beta^2 - \cos^2\Phi/2)^{1/2}}. \qquad \text{(A-9)}$$

In Eq. (A-9), β is the velocity of meson η, and $\gamma = 1/(1-\beta^2)^{1/2}$.

To get the second factor in Eq. (A-8), we must derive the relationship between Φ and δ. This can be easily done by applying energy and momentum conservation to the decay illustrated in Fig. 9-a. One finds

$$\beta\cos\delta = \cos\Phi/2. \qquad \text{(A-10)}$$

The desired result is

$$\frac{dn}{d(\cos\delta)} = \frac{-(1-\beta^2)\cos\delta}{(1-\cos^2\delta)^{1/2}\ (1-\beta^2\cos^2\delta)^{3/2}}. \qquad \text{(A-11)}$$

Or, writing $\mu = \cos\delta$, and putting in distribution (A-9),

$$\frac{d\sigma}{d\Omega_B} = \sum_\ell \left[C_\ell \int_{\frac{1}{\beta}\cos\frac{\Phi_{max}}{2}}^{1} \frac{(1-\beta^2)\mu\, P_\ell(\mu)d\mu}{(1-\mu^2)^{1/2}(1-\beta^2\mu^2)^{3/2}} \right] P_\ell(\cos\theta_B). \tag{A-12}$$

The limits of integration correspond to taking δ from 0 to some maximum angle, less than 90 deg, which is related by Eq. (A-10) to the maximum opening angle one wishes to consider when selecting events.

This is the result we seek. The integrals

$$\zeta_\ell = \int_{\frac{1}{\beta}\cos\frac{\Phi_{max}}{2}}^{1} \frac{(1-\beta^2)\,\mu\, P_\ell(\mu)d\mu}{(1-\mu^2)^{1/2}(1-\beta^2\mu^2)^{3/2}} \tag{A-13}$$

have been done numerically, resulting in Table A-I. These express the relationship between the coefficients of a Legendre polynomial expansion of the differential cross section for η production, namely C_ℓ, and the expansion coefficients of the γ-ray bisector distribution, given by $\zeta_\ell C_\ell = A_\ell$.

FOOTNOTES AND REFERENCES

*This work was supported in part by the U. S. Atomic Energy Commission at the Lawrence Radiation Laboratory (Berkeley) under Contract No. W-7405-eng-48 and at the University of Hawaii under Contract AT(04-3)-511.

†Present address: Oberlin College, Oberlin, Ohio.

‡Present address: California Institute of Technology, Pasadena, California.

**Present address: NASA Manned Spacecraft Center, Houston, Texas.

††Present address: University of Notre Dame, Notre Dame, Indiana.

‡‡Present address: University of Wisconsin, Madison, Wisconsin.

1. A. Pevsner, R. Kraemer, M. Nussbaum, C. Richardson, P. Schlein, R. Strand, T. Toohig, M. Block, A. Engler, R. Gessaroli, and O. Meltzer, Phys. Rev. Letters 7, 421 (1961).

2. G. Puppi, Ann. Rev. Nucl. Sci. 13, 287 (1963).

3. Pierre L. Bastien, J. Peter Berge, Orin I. Dahl, Massimiliano Ferro-Luzzi, Donald H. Miller, Joseph J. Murray, Arthur H. Rosenfeld, and Mason B. Watson, Phys. Rev. Letters 8, 114 (1962).

   Pierre L. Bastien, J. Peter Berge, Phys. Rev. Letters 10, 188 (1963).

4. P. Auvil, C. Lovelace, A. Donnachie, and A. T. Lee, Phys. Letters 12, 76 (1964).

5. P. Bareyre, C. Brickman, A. V. Stirling, and G. Villet, Phys. Letters 18, 342 (1965).

6. Robert J. Cence, Phys. Letters 20, 306 (1966).

7. B. H. Bransden, P. J. O'Donnell, and R. G. Moorhouse, Phys. Letters 11, 339 (1964).

8. L. David Roper, Robert M. Wright, and Bernard T. Feld, Phys. Rev. 138, B190 (1965).

9. Remarks on elementary resonance theory are found in Mason B. Watson, Massimiliano Ferro-Luzzi, and Robert D. Tripp, Phys. Rev. 131, 2248 (1963).

10. W. Bruce Richards, Charles B. Chiu, Richard D. Eandi, A. Carl Helmholz, Robert W. Kenney, Burton J. Moyer, John A. Poirier, Robert J. Cence, Vincent Z. Peterson, Narender K. Sehgal, and Victor J. Stenger, Bull. Am. Phys. Soc. 8, 603 (1963); ibid., 9, 409 (1964); Phys. Rev. Letters 16, 1221 (1966).

11. Walter B. Richards, Total and Differential Cross Sections for $\pi^- p \to \eta n$ from Threshold to 1300 MeV (Ph. D. Thesis), Lawrence Radiation Laboratory Report UCRL-16195, Nov. 1965 (unpublished).

12. R. J. Cence, V. Z. Peterson, V. J. Stenger, C. B. Chiu, R. D. Eandi, A. C. Helmholz, R. W. Kenney, B. J. Moyer, J. A. Poirier, and W. B. Richards, Phys. Rev. Letters 19, 1393, 1967.

13. Charles B. Chiu, Richard D. Eandi, A. Carl Helmholz, Robert W. Kenney, Burton J. Moyer, John A. Poirier, W. Bruce Richards, Robert J. Cence, Vincent Z. Peterson, Narender K. Sehgal, and Victor J. Stenger, Phys. Rev. 156, 1415 (1967).

14. Charles Bin Chiu, Pion-Proton Charge-Exchange Scattering, 500 to 1300 MeV (Ph. D. Thesis), Lawrence Radiation Laboratory Report UCRL-16209, Nov. 1965 (unpublished).

15. Gunnar Källén, Elementary Particle Physics (Addison Wesley Publishing Co., Inc., Reading, Massachusetts, 1964), p. 32.

16. N. Barash-Schmidt, A. Barbaro-Galtieri, L. R. Price, A. H. Rosenfeld, P. Söding, C. G. Wohl, M. Roos, and G. Conforto, Rev. Mod. Phys. 41, 109 (1969).

17. L. Bertanza, P. L. Connolly, B. B. Culwick, F. R. Eisler, T. Morris, R. Palmer, A. Prodell, and N. P. Samios, Phys. Rev. Letters 8, 332 (1962).

18. Brandeis-Brown-Harvard-M. I. T. -Padova Collaboration, Phys. Rev. Letters 13, 486 (1964).

19. W. H. Jones, D. M. Binnie, A. Duane, J. P. Horsey, D. C. Mason, J. A. Newth, I. U. Rahman, J. Walters, N. Horwitz, and P. Palit, Phys. Letters 23, 597 (1966).

20. P. Auvil and C. Lovelace, πp Phenomenology, 300—1300 MeV, Physics Department, Imperial College, London, Report ICTP/64/37 (1964) (unpublished).

21. C. Lovelace, "Nucleon Resonances and Low Energy Scattering", rapporteur talk at the Heidelberg International Conference on Elementary Particles, September 1967, pp. 79-116 of Proceedings. This paper contains an extensive bibliography and summary of existing pion-nucleon phase-shift analyses.

22. F. Uchiyama-Campbell, Phys. Letters 18, 189 (1965).

23. Peter N. Dobson, Jr., Phys. Rev. 146, 1022 (1966).

24. James S. Ball, Phys. Rev. 149, 1191 (1966); James S. Ball and William R. Frazer, Phys. Rev. Letters 7, 204 (1961).

25. A. W. Hendry and R. G. Moorhouse, Phys. Letters 18, 171 (1965).

26. F. Uchiyama-Campbell and R. K. Logan, Phys. Rev. 149, 1220 (1966).

27. William R. Frazer and Archibald W. Hendry, Phys. Rev. 134, B1307 (1964).

28. A. T. Davies and R. G. Moorhouse, Nuovo Cimento 52A, 1112 (1967).

29. T. A. Moss, Phys. Rev. 163, 1785 (1967).

30. R. D. Tripp (Lawrence Radiation Laboratory) private communication, and Nucl. Phys. B3, 10 (1967).

31. A. E. Brenner (Harvard University), private communication, 1969.

32. J. D. Jackson, Classical Electrodynamics (John Wiley and Sons, Inc., New York, 1962), p. 69.

Table I. Opening angles of eta region.

T_{π^-} (MeV)	Lower limit accepted for eta region (deg)	Theoretical min. opening angle (deg)	Upper limit accepted for eta region (deg)	Theoretical fraction of events included (%)
592	152	156.1	168	87
655	136	139.4	154	78
704	126	130.9	148	78
875	106	111.6	134	78
975	100	103.9	126	76
1117	92	95.5	120	77
1300	84	87.2	110	75

Table II. Ratio r and partial η production cross section.

T_{π^-} (MeV)	Fraction of events in η region due to background (%)	Total number of etas	$(\chi^2/d)^{1/2}$	r (%)	$f_\eta \sigma (\pi^- p \to \eta n)$ (mb)
592	8	258 ± 20	1.190	7.8±0.06	0.60 ± 0.06
655	11	693 ± 35	1.027	17.1 ± 0.9	0.93 ± 0.08
704	14	767 ± 38	0.955	19.5 ± 1.1	0.93 ± 0.08
875	30	246 ± 29	0.992	6.4 ± 0.8	0.41 ± 0.06
975	21	420 ± 36	1.093	15.5 ± 1.4	0.46 ± 0.06
1117	15	523 ± 38	1.167	20.7 ± 1.6	0.45 ± 0.05
1300	23	484 ± 44	1.089	11.8 ± 1.1	0.25 ± 0.03

Table III. Differential partial cross section $\frac{d\sigma_\eta(2\gamma)}{d\Omega} = f_\eta \frac{d\sigma}{d\Omega}(\pi^- p \to \eta n)$ in μb/sr. Errors do not include the error of normalization because the differential cross section relative shapes are known more accurately than are the absolute values of the points. Normalization errors, $\Delta_T(\%)$, are given in units of percent at each energy and are to be converted to μb/sr and added in quadrature to the tabulated errors to find the complete absolute errors.

$$f_\eta = \frac{\Gamma(\eta \to 2\gamma)}{\Gamma(\eta \to \text{all decays})} .$$

	$\cos\theta_B$										
T_π^- (MeV)	0.9	0.7	0.5	0.3	0.1	-0.1	-0.3	-0.5	-0.7	-0.9	Δ_T (%)
592	54±13	70±16	52±13	45±15	36±12	53±14	47±13	35±11	41±11	44±13	10
655	116±15	82±12	60±12	51±11	77±12	64±11	61±11	56±11	71±12	100±13	9
704	136±15	98±13	85±13	63±11	65±10	71±11	60±11	47±10	57±11	61±12	9
875	49±12	51±14	36±13	45±11	31±12	22±10	17±9	15±9	17±9	44±11	14
975	63±10	87±12	71±11	58±10	44±9	22±7	14±6	1±6	6±6	0±5	13
1117	54±9	69±10	64±9	55±9	40±8	33±6	19±5	14±5	4±6	7±5	11
1300	42±6	49±6	40±6	30±6	21±4	6±4	2±3	0±3	4±3	4±3	12

Table IV. Coefficients of Legendre polynomial expansion of η differential partial cross section $\frac{d\sigma_\eta(2\gamma)}{d\Omega} = f_\eta \frac{d\sigma}{d\Omega}(\pi^- p \to \eta n)$.

$$f_\eta = \frac{\Gamma(\eta \to 2\gamma)}{\Gamma(\eta \to \text{all decays})}.$$

T_{π^-} (MeV)	A_0 (μb/sr)	A_1 (μb/sr)	A_2 (μb/sr)	A_3 (μb/sr)	A_4 (μb/sr)
592	46 ± 5				
655	73 ± 7	7 ± 8	49 ± 14		
704	74 ± 7	38 ± 6	36 ± 9		
875	33 ± 5	16 ± 3	19 ± 5	-34 ± 9	
975	36 ± 5	52 ± 4	1 ± 6	-33 ± 9	
1117	36 ± 4	39 ± 2	- 6 ± 3	-26 ± 5	
1300	20 ± 3	31 ± 1	9 ± 2	-21 ± 3	-20 ± 4

Table V. Number of events after full-empty subtractions.

T_π-lab (MeV)	Number of showers					
	1	2	3	4	5	6
500	4563	8203	1240	524	59	6
533	2814	4966	768	321	31	4
592	1885	4466	752	537	133	41
655	2371	6730	1755	1215	382	112
704	2768	6373	2215	1471	384	126
875	1910	6107	2027	1415	360	97
975	1927	4841	1662	1138	293	90
1117	1172	4461	1893	1591	580	233
1300	1473	6486	2702	2471	802	389

Table A-I. Values of ζ_ℓ at the energies of this experiment.

	T_{π^-} (MeV)						
	592	655	704	875	975	1117	1300
β_η (c.m.)	0.2067	0.3468	0.4155	0.5622	0.6161	0.6724	0.7241
Φ_{max} (deg)	168	154	148	134	126	120	110
ζ_0	0.8675	0.7811	0.7785	0.7811	0.7587	0.7721	0.7451
ζ_1	0.7439	0.6998	0.7016	0.7137	0.7024	0.7178	0.7026
ζ_2	0.5489	0.5618	0.5701	0.5963	0.6021	0.6207	0.6249
ζ_3	0.3557	0.4059	0.4193	0.4571	0.4791	0.5005	0.5250
ζ_4	0.2190	0.2698	0.2845	0.3261	0.3568	0.3794	0.4182
ζ_5	0.1528	0.1769	0.1888	0.2252	0.2545	0.2762	0.3192
ζ_6	0.1372	0.1309	0.1380	0.1632	0.1832	0.2019	0.2388
ζ_7	0.1466	0.1201	0.1227	0.1363	0.1439	0.1585	0.1822

FIGURE CAPTIONS

Fig. 1. Experimental arrangement. Six spark chambers form the walls of a cubical box. A_{0-9} are anti-counters. M_1, M_2, M_3 are π^- monitor counters.

Fig. 2. Experimental opening-angle distribution for $T_{\pi^-} = 1300$ MeV. The inset shows the region of the η peak with an expanded vertical scale. Events were chosen from the region between the vertical lines for the η differential cross section.

Fig. 3. Components of the background subtraction at $T_{\pi^-} = 1300$. Shown in the histograms are the actual number of events used in the subtraction from the opening-angle distribution of Fig. 2.

Fig. 4. Partial η production cross section $\sigma_\eta(2\gamma) = \sigma(\pi^- p \to \eta n;\ \eta \to 2\gamma)$ as a function of pion kinetic energy. The curves are due to Ball (Ref. 24) (-·-·-), Dobson (Ref. 23) (---), and Hendry and Moorhouse (Ref. 25) (——). Some low-energy data of Ref. 18 are shown for comparison ($\overset{\mathrm{I}}{\Delta}$).

Fig. 5. Partial differential cross section for η production. The dotted line is the best fit to the bisector-distribution data points, and the solid line is the η differential cross section.

Fig. 6 a, b. Legendre polynomial expansion coefficients of the η differential partial cross section. The errors shown do not include the overall normalization error at each energy.

Fig. 7 a, b. $(\chi^2/d)^{1/2}$ versus order of fit for the differential partial cross-section expansion at each energy. The heavy dot carries a momentum label and shows the order of fit used in each case.

Fig. 8. Total cross sections for neutral final states in $\pi^- p$ collisions. From Ref. 13 and from Review of Particle Properties, Lawrence Radiation Laboratory Report UCRL-8030 Rev., Jan. 1969.

Fig. 9. a. Angles used in the kinematical equations.

b. Coordinate system for integration of bisector equation.

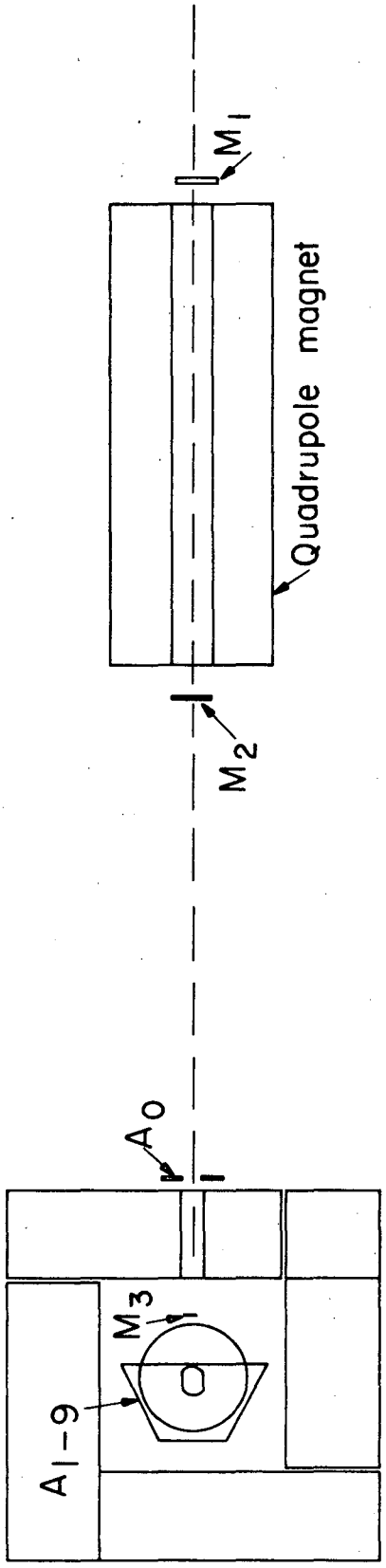

Fig. 1

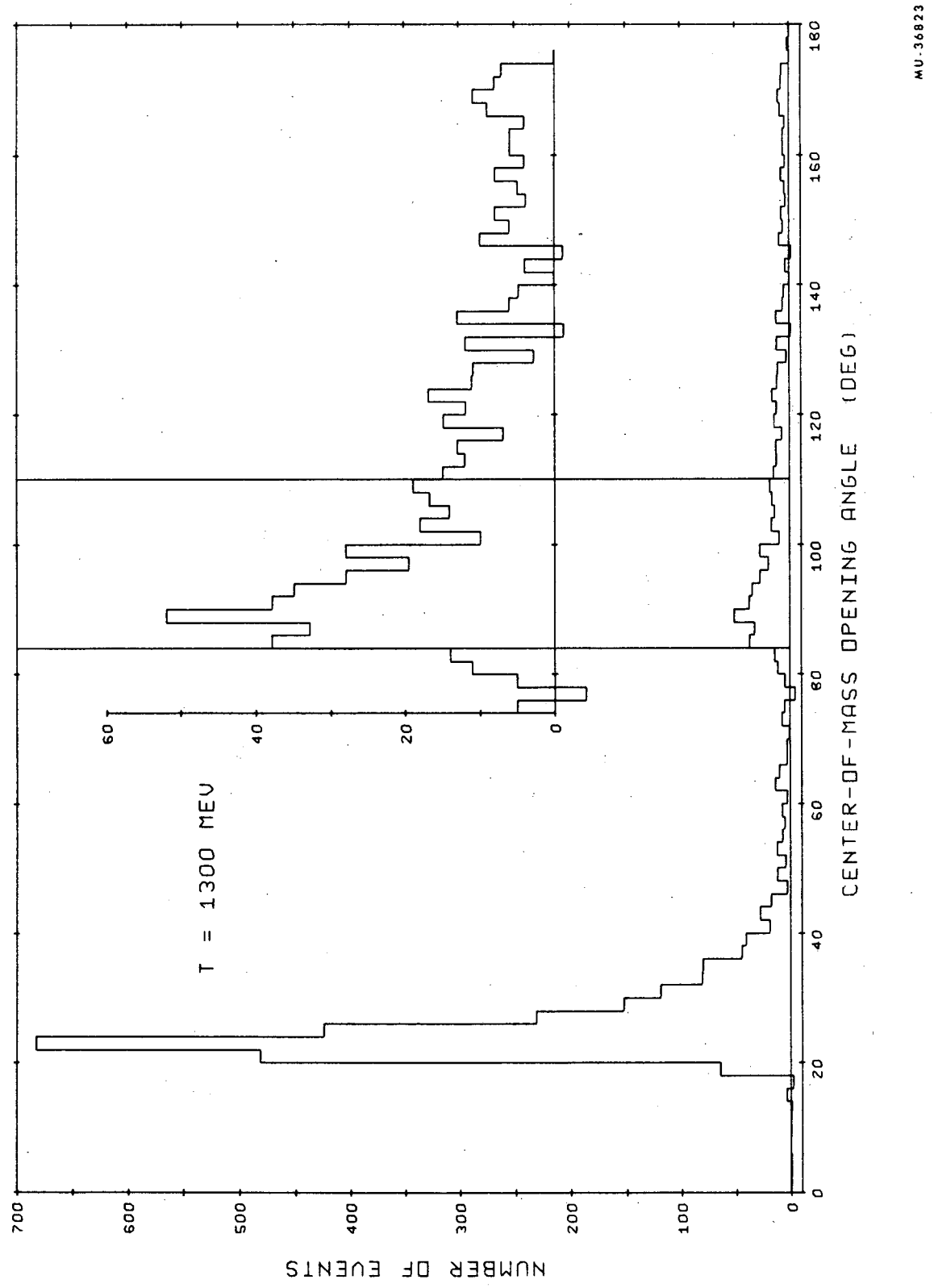
MU-36823
NUMBER OF EVENTS
CENTER-OF-MASS OPENING ANGLE (DEG)
T = 1300 MEV
0
100
200
300
400
500
600
700
0
20
40
60
80
100
120
140
160
0
20
40
60

Fig. 2

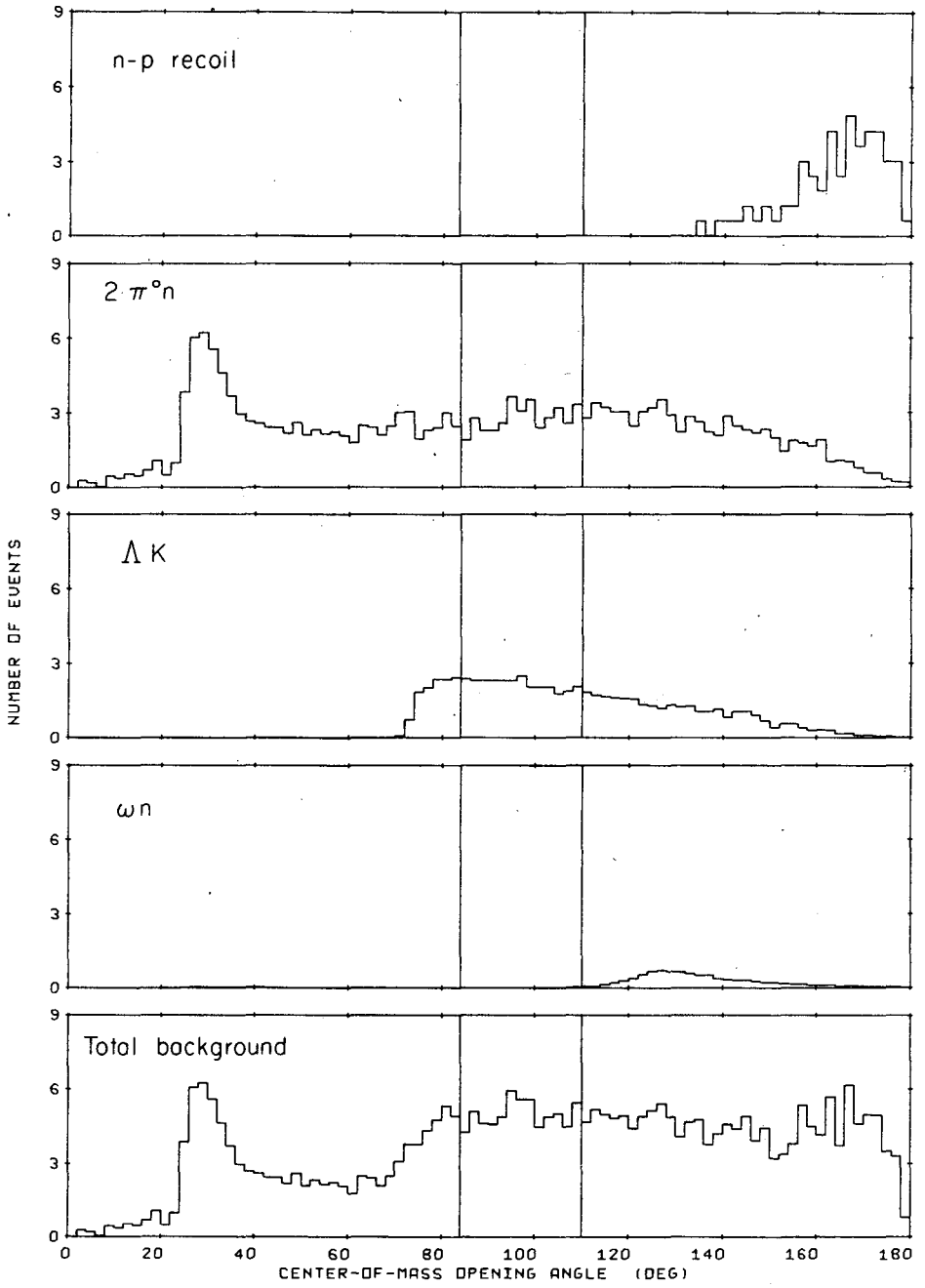
n-p recoil
2 π°n
Λ K
ωn
Total background
NUMBER OF EVENTS
0
3
6
9
0
20
40
60
80
100
120
140
160
180
CENTER-OF-MASS OPENING ANGLE (DEG)
MUB-6545

Fig. 3

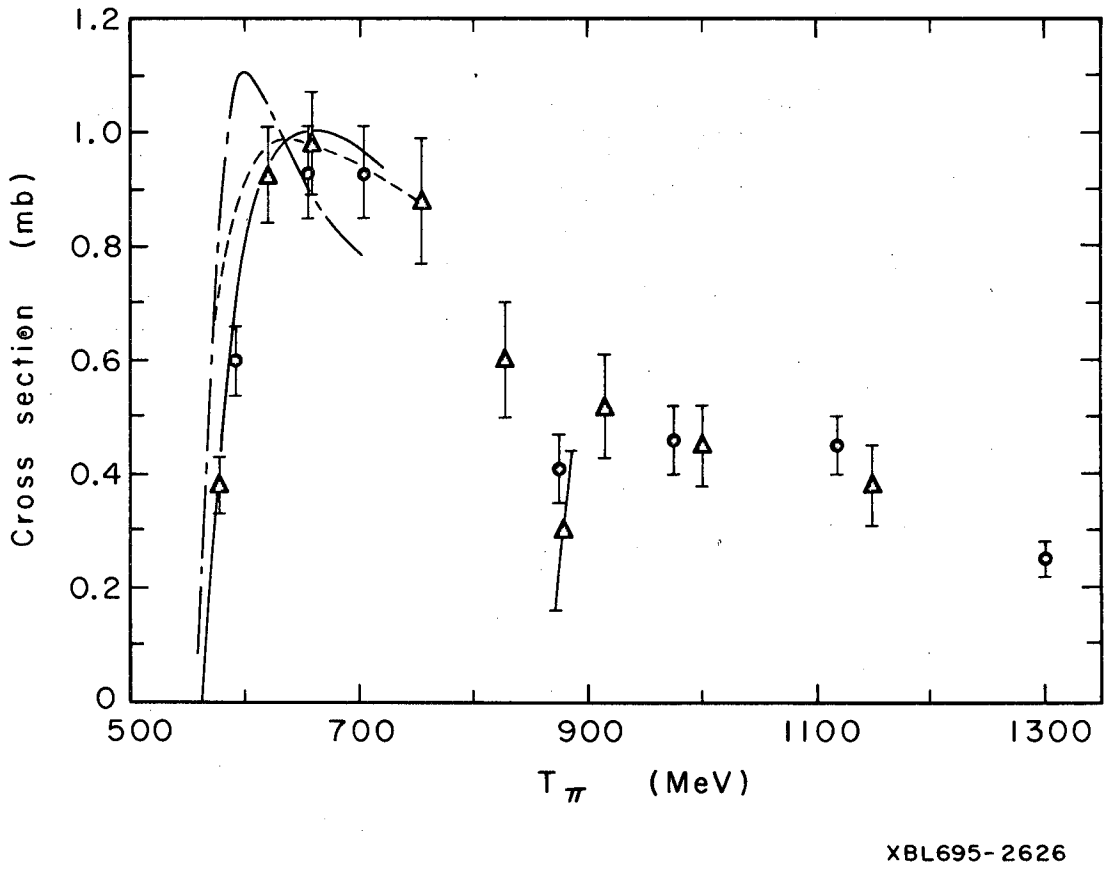
1.2
1.0
0.8
0.6
0.4
0.2
0
Cross section (mb)
500
700
900
1100
1300
T_π (MeV)
XBL695-2626

Fig. 4

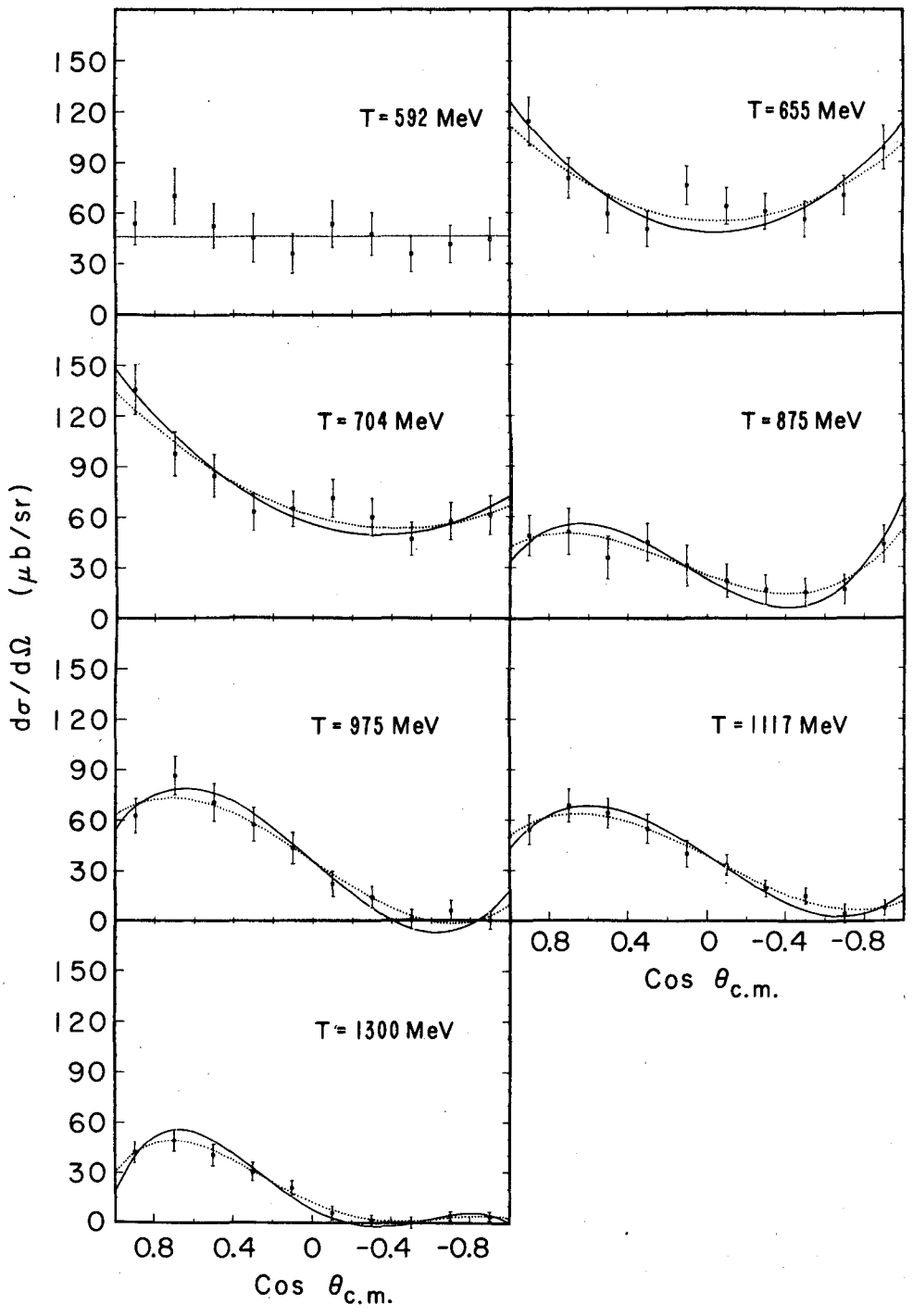
T = 592 MeV
T = 655 MeV
T = 704 MeV
T = 875 MeV
T = 975 MeV
T = 1117 MeV
T = 1300 MeV
dσ/dΩ (μb/sr)
Cos θc.m.
0.8 0.4 0 -0.4 -0.8
150
120
90
60
30
0

Fig. 5

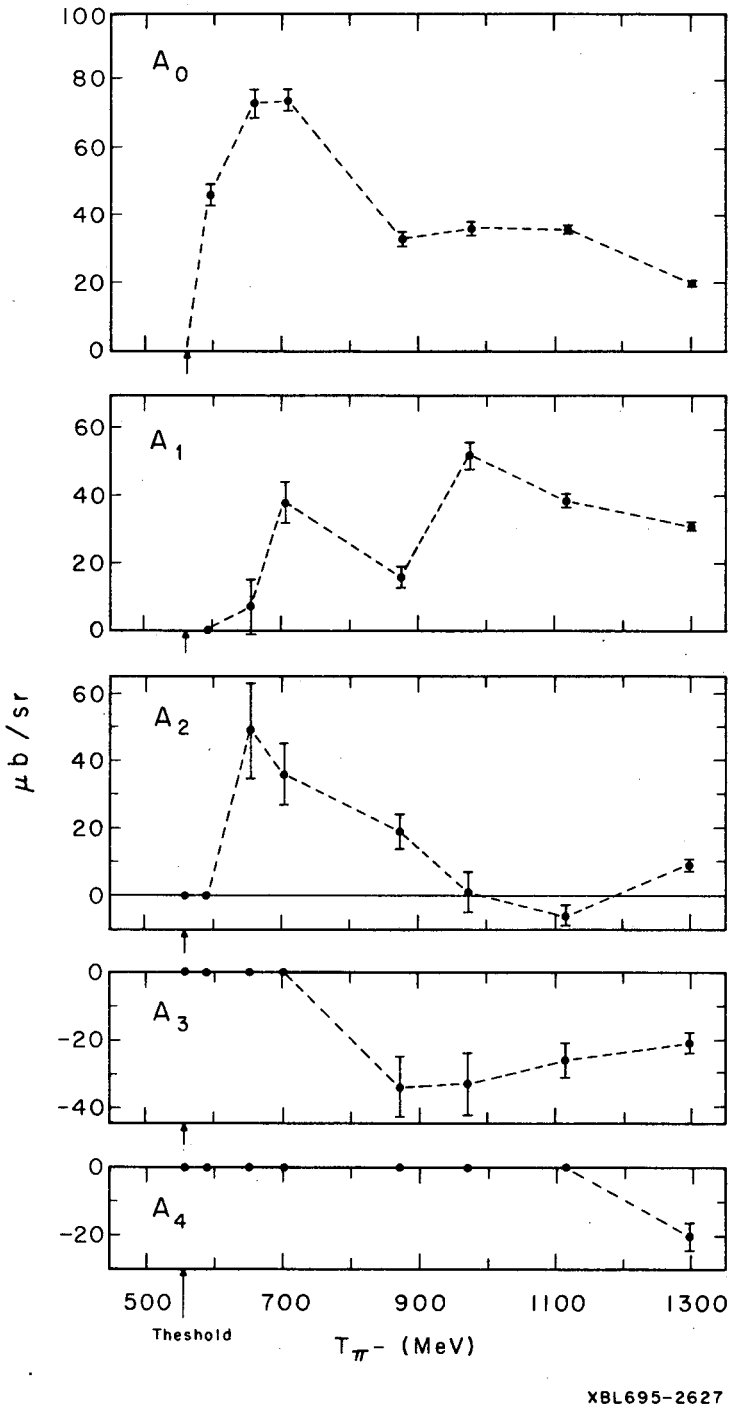

Fig. 6

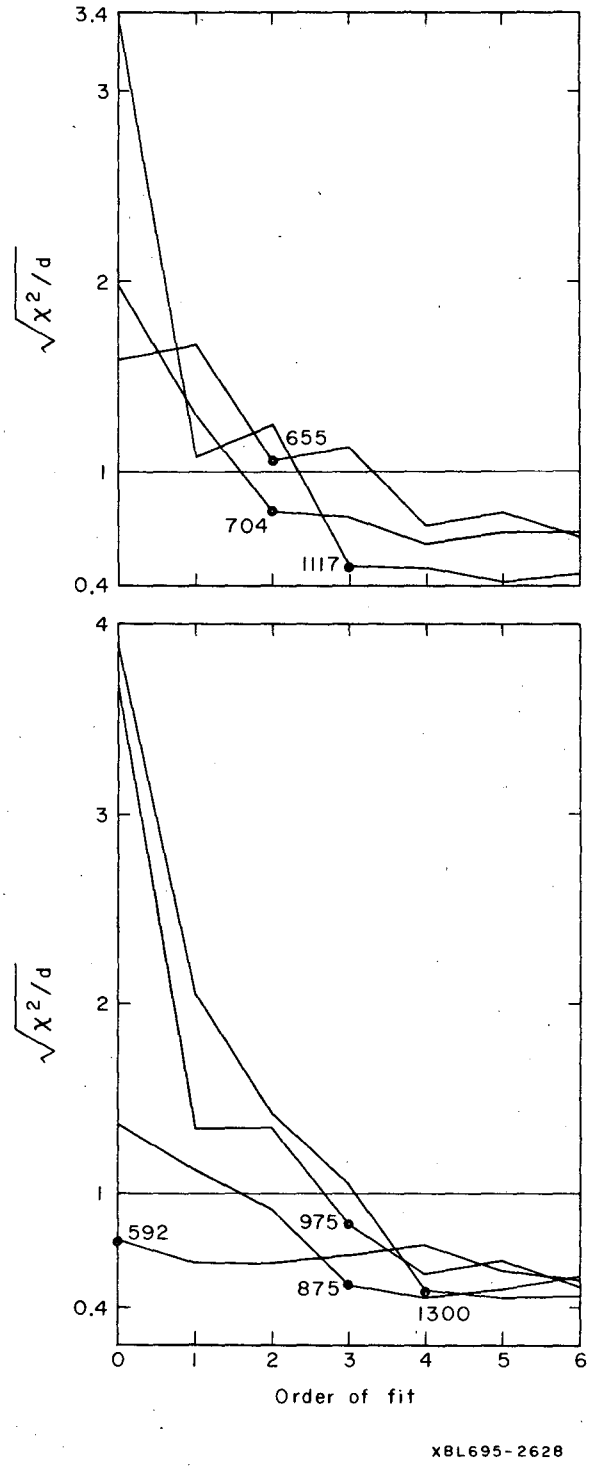
3.4
3
2
1
0.4
$\sqrt{\chi^2/d}$
655
704
1117
4
3
2
1
0.4
$\sqrt{\chi^2/d}$
592
975
875
1300
0
1
2
3
4
5
6
Order of fit
XBL695-2628

Fig. 7

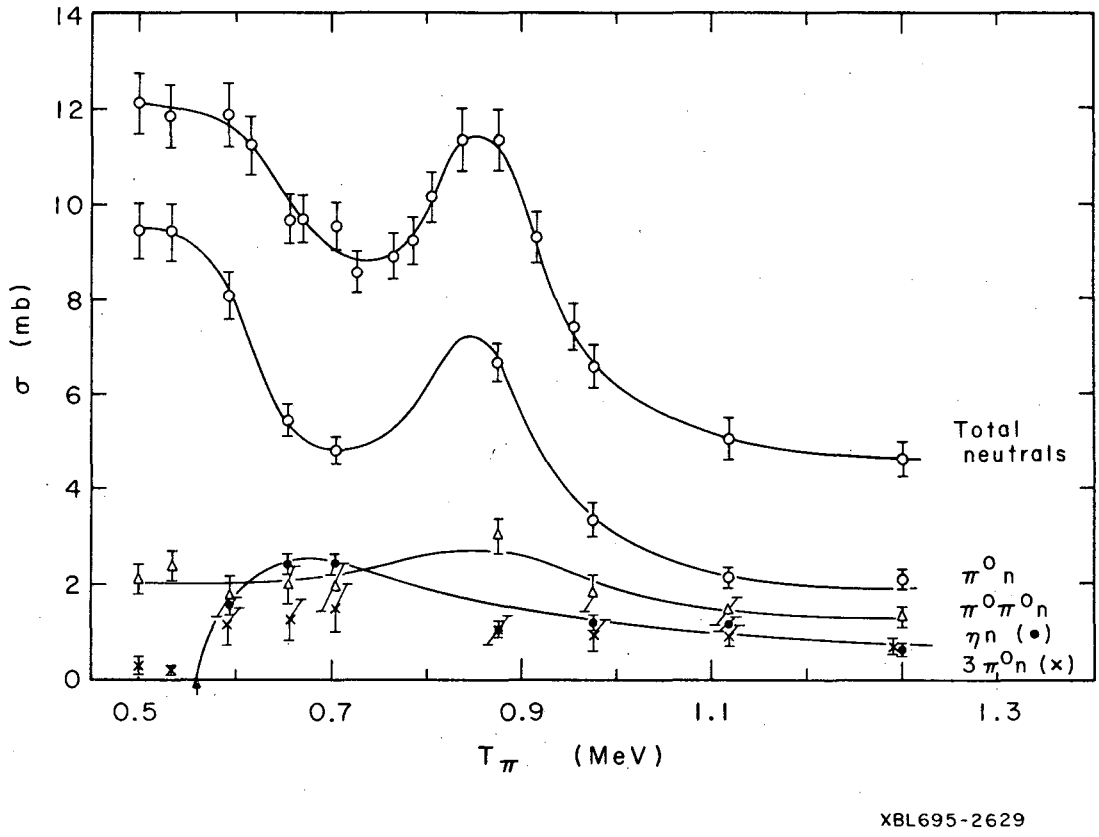
14
12
10
8
6
4
2
0
σ (mb)
0.5
0.7
0.9
1.1
1.3
T_π (MeV)
Total neutrals
$\pi^0 n$
$\pi^0\pi^0 n$
ηn (•)
$3\pi^0 n$ (×)
XBL695-2629

Fig. 8

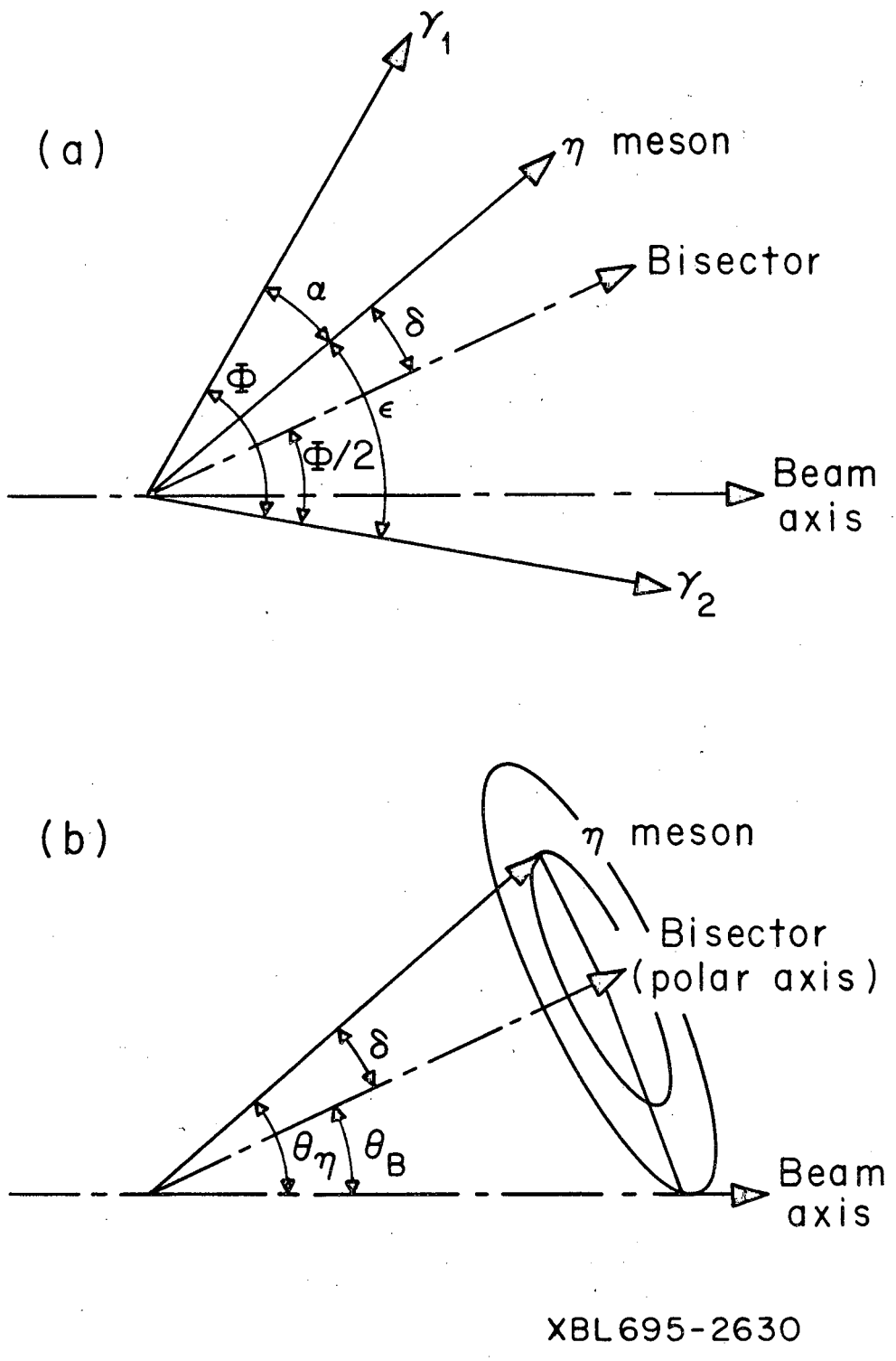
(a)
γ_1
η meson
Bisector
α
δ
Φ
ϵ
$\Phi/2$
Beam axis
γ_2
(b)
η meson
Bisector
(polar axis)
δ
θ_η
θ_B
Beam axis
XBL695-2630

Fig. 9

TECHNICAL INFORMATION DIVISION
LAWRENCE RADIATION LABORATORY
UNIVERSITY OF CALIFORNIA
BERKELEY, CALIFORNIA 94720